Thermally-induced ratcheting of a thermo-active reinforced concrete pile in sand under sustained lateral load

Rui Zhao[1]; *Anthony Kwan Leung[2]; Jonathan Adam Knappett[3]

Abstract

Thermally-induced ratcheting of a thermo-active pile is the accumulation of net and irreversible pile head displacement upon heating–cooling cycles. Although this kind of phenomenon has been observed in vertically-loaded piles in sand, it is unknown whether this exists in laterally-loaded cases, and also what underlying mechanisms occur under the thermomechanical flexural soil-pile interaction. This study presents a series of centrifuge tests and finite-element simulations of the thermomechanical behaviour of a laterally-loaded thermo-active pile in sand. A new model reinforced concrete (RC) was used in the centrifuge tests to realistically mimic the thermal and mechanical properties of a prototype RC pile. Ratcheting was evident in laterally-loaded piles and its extent was more significant when the working horizontal load is higher. The ratcheting phenomenon was attributed to the accumulation of soil plastic strain due to the cyclic mechanical loading induced by pile thermal horizontal expansion and contraction, soil dilation upon soil-pile interface shearing, and creep. The additional bending moment induced by the thermal action did not induce yielding within the pile. A subsequent numerical sensitivity study suggested that ignoring the softening behaviour of the sand would lead to underestimation of the magnitude of the accumulative thermally-induced pile head lateral displacement.

Keywords: Centrifuge modelling; Finite-element modelling; Piles; Temperature effects

[1] Postdoctoral Researcher, Center for Hypergravity Experiment and Interdisciplinary Research, Zhejiang University, Hangzhou

[2] Assistant Professor, Department of Civil and Environmental Engineering, Hong Kong University of Science and Technology, Hong Kong SAR

[3] Professor, Division of Civil Engineering, School of Science and Engineering, University of Dundee, Dundee

*Corresponding author; E-mail: ceanthony@ust.hk

Introduction

A thermo-active pile is an energy geostructure (Brandl, 2006) that has been increasingly used in practice for supporting and reducing carbon emissions from buildings or other infrastructure (Bourne-Webb et al., 2009; Mimouni and Laloui, 2015). In such applications, the pile is normally made of reinforced concrete (RC) in which heat-circulating pipes of different geometries and configurations are embedded during casting to allow heat exchange with the surrounding soil (Loveridge and Powrie, 2013). Depending on the application, the pile may be mechanically subjected to predominantly vertical loading due to a supported superstructure, horizontal loading if used in a bridge abutment or embankment stabilisation, or combined vertical-horizontal (and potentially moment too) in buildings subjected to pile eccentricity. In addition to these mechanical actions, thermal loading will occur upon repeated heating-cooling cycles. The complex thermomechanical loading conditions and the associated interaction between the pile and the surrounding soil could substantially affect the capacity (e.g., Goode and McCartney, 2015) and serviceability (e.g., Ng et al., 2016a) of the soil-pile system.

In the last decade, studies have been conducted to experimentally and numerically study the behaviour of thermo-active piles (e.g., Goode and McCartney, 2015; Ng et al., 2016b; Gawecka et al., 2017) and pile groups (e.g., Mimouni and Laloui, 2015; Di Donna et al., 2016). The centrifuge modelling technique (e.g., Taylor, 1995) has been recognised as an effective means to investigate thermomechanical soil-pile interaction (Rotta Loria et al., 2015a; Ng et al., 2019). This technique enables small-scale physical models to be tested within an elevated gravity (g) field, such that the soil effective stress levels are the same as those experienced within much larger prototypes at homologous points. In this kind of model test, RC energy piles have traditionally been modelled by an elastic aluminum cylinder (e.g., Ng et al., 2016a) or by concrete with the use of the actual size of aggregates (e.g., Goode and McCartney, 2015). Either way cannot simultaneously model the pile's nonlinear, quasi-brittle mechanical properties, thermal properties and also the process of heat exchange between the pile and the surrounding soil (Zhao et al., 2020). Zhao et al. (2020) developed a plaster-based mortar to simulate thermomechanical prototype properties, building on the pioneering work of Knappett et al. (2011). Zhao et al. (2020) showed that a model RC pile produced by this new material could effectively capture most of the key features of a vertically-loaded thermo-active pile at 1 g when compared to those reported from existing large- or full-scale experiments. The application of this appealing model material has never been attempted under high g condition.

Pile ratcheting is a phenomenon that describes the net and irreversible accumulation of pile displacement associated with repeated/cyclic loading. Thermally-induced pile ratcheting, in particular, is referred to as the net pile head displacement due to repeated heating and cooling cycles. Such behaviour has been observed in vertically-loaded piles via physical model tests at 1 g (Nguyen et al., 2017; Tang et al., 2014) and also at high g (Ng et al., 2014; Ng et al., 2016a) in both clay and sand. Further numerical analysis (Ng et al., 2016b) implied that the underlying mechanism of thermally-induced pile head ratcheting in the axial direction is attributed to the contraction of sand due to repeated thermal expansion and contraction of the pile. Most studies focused on the behaviour of vertically-loaded piles. As far as the authors are aware, there is no study on thermally-induced ratcheting for laterally-loaded piles. It is unknown whether any such ratcheting would mobilise additional pile shear force and bending moment, and if so, by how much. Because of a lack of physical data on the thermomechanical behaviour of laterally-loaded pile, any numerical modelling method developed for this problem cannot be validated.

The objective of this study was to conduct a series of centrifuge model tests and performed finite-element (FE) simulations of the thermomechanical behaviour of a laterally-loaded RC pile in sand and then to reveal the underlying governing mechanisms. The small-scale model RC developed by Zhao et al. (2020) was used to produce the model RC piles for capturing their thermomechanical properties in the centrifuge. The test results were used to compare with FE simulations that considered the RC pile to be elasto-plastic while the sand was modelled to incorporate the effects of small-strain nonlinearity and large-strain, post-peak strain-softening phenomena. The FE model was finally used to conduct sensitivity analyses to identify influential factors that govern the thermally-induced ratcheting behaviour of a laterally-loaded pile.

Centrifuge modelling

Similitude relationships and scaling laws

The centrifuge modelling technique can recreate the stress conditions in a 1:N scale model that would exist in the prototype, by increasing the 'gravitational' acceleration N times in a centrifuge (Taylor, 1995). To correctly model the lateral thermomechanical behaviour of thermo-active pile in the centrifuge, non-dimensional groups were identified as outlined below.

Upon pile thermal loading, the major heat transfer mechanism in dry soil is conduction since water is absent for any convection. In this case, the Fourier Number, which is defined as the ratio of heat conduction rate to the rate of thermal energy storage, may be considered as a non-dimensional group to describe the duration of heat transfer:

$$\left(\frac{\alpha t}{r^2}\right)_{model} = \left(\frac{\alpha t}{r^2}\right)_{prototype} \quad (1)$$

where α is the soil thermal diffusivity (dimensions $[L^2/T]$) which is defined as $\lambda/\rho C_s$; λ is the soil thermal conductivity $[MLT^{-3}\Theta^{-1}]$; ρ is the soil density $[ML^{-3}]$; C_s is the soil specific heat capacity $[\ L^2T^{-2}\ \Theta^{-1}]$; t is the characteristic time $[T]$; r is the radial distance away from the heat source $[L]$; and the subscripts $model$ and $prototype$ denote model and prototype scale, respectively. Considering the same soil material in model and prototype (i.e., $\alpha_{model} = \alpha_{prototype}$) and the geometrical scaling of r (i.e., $N \cdot r_{model} = r_{prototype}$), the heat conduction time is scaled by N^2. This means that a greater volume of soil would be thermally affected in the centrifuge than in a prototype (Ng et al., 2015; Goode and McCartney, 2015). However, since the mechanical properties of the silica sand being tested in this study were not sensitive to temperature changes below 100 ˚C (Ng et al., 2016c), this condition was deemed negligible.

Both the soil and pile thermal expansion upon heating and contraction upon cooling were assumed to be elastic and therefore controlled by the respective coefficient of linear thermal expansion (i.e., CTE_{soil} and CTE_{pile}). These coefficients are non-dimensional and since the same soil materials were considered in both model and prototype scale, no scaling was needed.

When an elastic pile embedded in an elastic homogenous soil is subjected to a lateral load at the pile head, the following non-dimensional group may be used (Wood, 2004):

$$\left(\frac{G \cdot L^4}{EI}\right)_{model} = \left(\frac{G \cdot L^4}{EI}\right)_{prototype} \quad (2)$$

where G is the soil shear modulus $[ML^{-1}T^{-2}]$; L is the pile length $[L]$; E is the pile Young's modulus $[ML^{-1}T^{-2}]$ and I is the second moment of inertia of the pile section $[L^4]$. Under an elevated g condition, the scaling factor for G is 1 if the same soil is considered in the model and prototype (Wood, 2004), while L and EI should be geometrically scaled by N and N^4, respectively. Other scaling laws relevant to the problem of interest are summarised in Table 1.

Test plan

In total, three centrifuge model tests were conducted using the 3.5-m-radius geotechnical beam centrifuge at the University of Dundee (Brennan et al., 2014). The first test was a reference push over test (denoted as RP), which was to determine the full lateral force-displacement curve of a 1:35 scale RC pile in dry sand. The next two tests (TP21 and TP73) were to study the thermo-mechanical behaviour of the similar piles, also in dry sand, by subjecting them to similar cyclic thermal loading patterns while under different maintained lateral loads. The lateral loads applied in tests TP21 and TP73 were 21% and 73% of the lateral capacity determined

from the RP test, respectively. These two tests aimed to study how different mobilised pile lateral force affected the magnitude of thermally-induced pile head displacement.

Table 1. Summary of relevant scaling factors (i.e., N = prototype/model, equal to 35 for both Tests D and S) for flexural soil-structure interaction problems in high-g (after Iai et al., 2005).

Quantity	Scale factor
Mechanical properties	
Length	N
Density	1
Stress	1
Strain	1
Stiffness (of soil)	1
Bending stiffness (E_pI_p)	N^4
Bending moment (M_{ult})	N^3
Force	N^2
Displacement	N
Thermal properties	
Temperature	1
Thermal diffusivity	1
Time (heat diffusion)	N^2
Coefficient of thermal expansion	1

Centrifuge model package

Figure 1 shows the centrifuge model setup used for test RP. An actuator driven by a servo motor was fixed at one end of the model box, which could apply a constant displacement rate up to 3.1 mm/s (model scale) during the test. A load cell was employed to measure the pile head load. On the opposite end of the box, a stainless steel draw-wire potentiometer was used to measure the pile head lateral displacement.

The schematic setup used for tests TP21 and TP73 is depicted in Fig. 2. The model package had two chambers. The first one was the test chamber (right-hand-side in the figure). The other chamber was for storing a load-controlled system for applying a maintained lateral load to the pile head. This consisted of a fixed mass on a wire, sitting on a platform supported by a linear actuator. During centrifuge spin-up, the mass was supported to prevent application of lateral load. Once up to speed, the actuator was lowered to apply the load. Through a pulley system, tension was transferred to the pile head through the wire with an in-line load cell, inducing a constant lateral load. Pile head lateral displacement was measured by the draw-wire potentiometer. From this point onwards, all values are expressed at prototype scale at N = 35, unless otherwise stated.

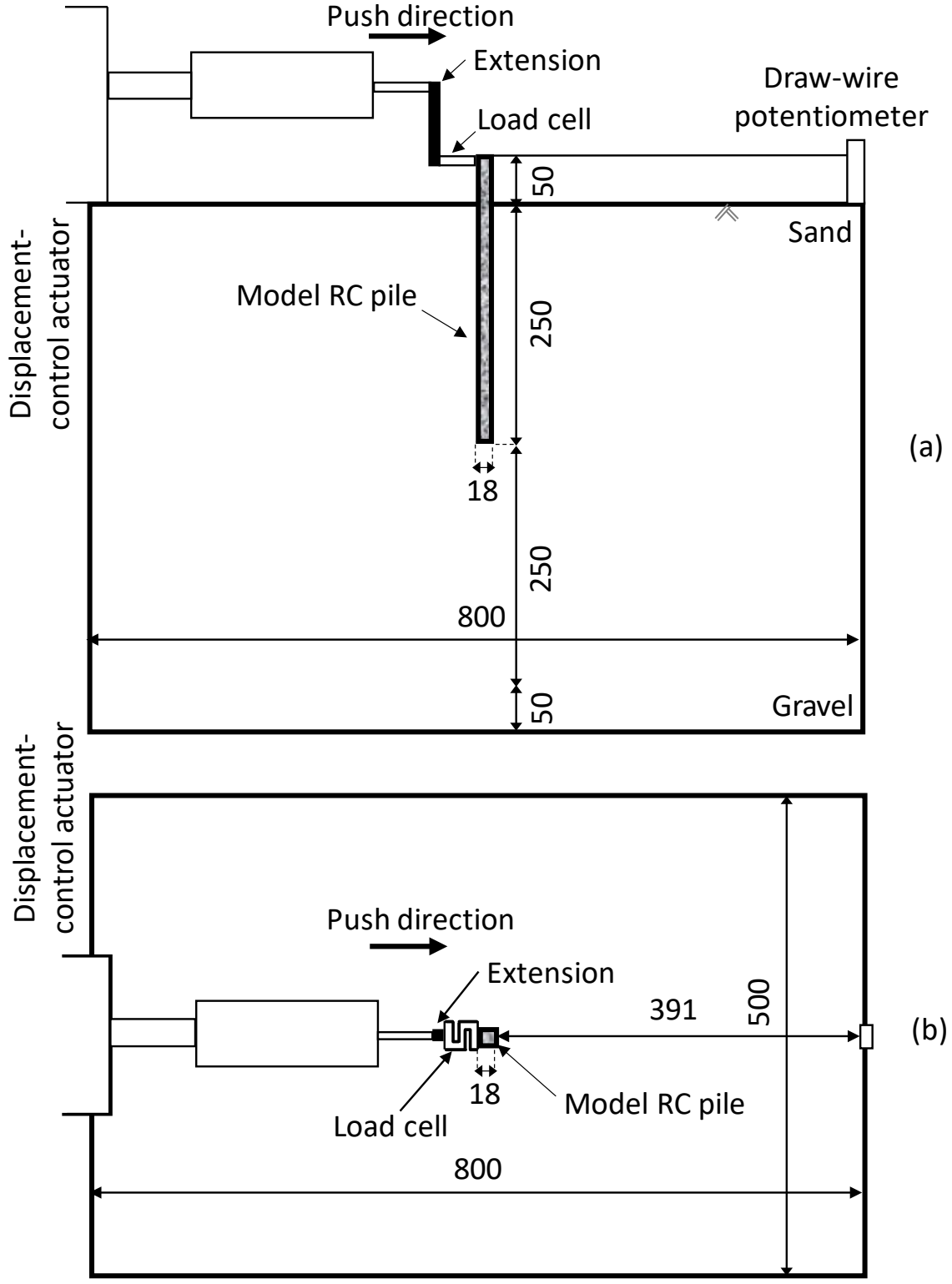

144 **Figure 1.** (a) Elevation and (b) plan views of the centrifuge model setup for the reference test
145 RP; all units are in millimetre (in model scale)
146

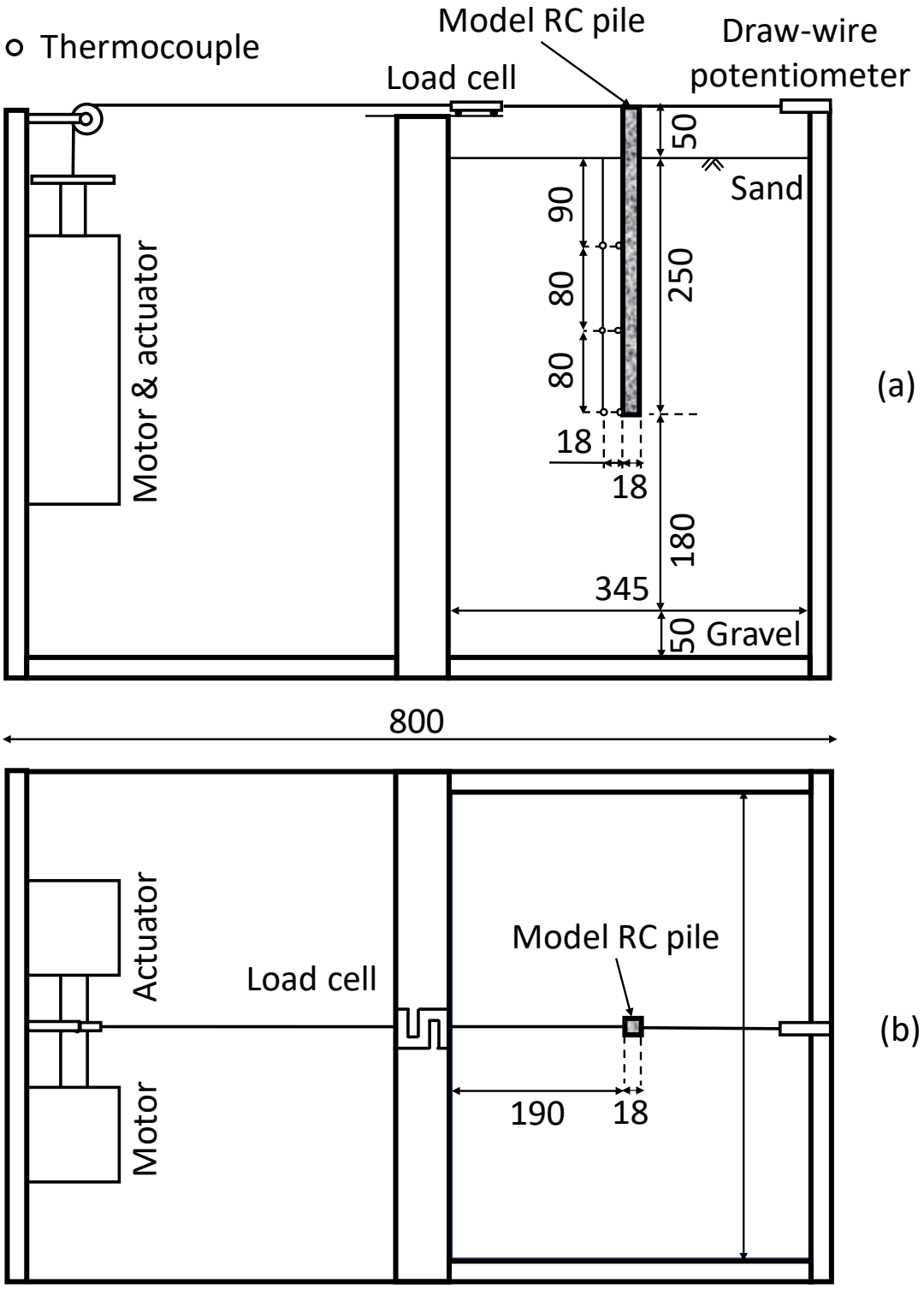

148 **Figure 2.** (a) Elevation and (b) plan views of the centrifuge model setup for tests TP21 and
149 TP73; all units are in millimetre (in model scale)

150

151 *Model RC thermo-active pile and instrumentation*

152 The model RC pile was fabricated using the model concrete originally developed by Knappett
153 et al. (2011) with a mixture of plaster, fine sand and water ratio of 1:1:0.9, as later modified by

Zhao et al. (2020). The latter added 6% (by volume) of copper powder to the mix to carefully adjust its thermal properties (both thermal conductivity and thermal expansion coefficient) while not detrimentally affecting compressive or flexural properties. Subsequently, the model concrete was used to create a 1:35 scale model RC pile as shown in Fig. 3. The pile was square in section and had a width (D) of 0.63 m and a length of 10.5 m. Four 35 mm diameter longitudinal reinforcing wires were used, resulting in a reinforcement ratio (by area) of 1.0%. Ten 22 mm diameter transverse shear links with a uniform spacing were used to form a cage and to fix two flexible silicone pipes within the cage. The silicone pipes were arranged in U-loops for circulating water in and out of the model RC pile during a centrifuge test. Based on four-point bending (FPB) tests reported by Zhao et al. (2020), the moment capacity (M_{ult}) and bending stiffness (E_pI_p; where $E_p$and I_p are the Young's modulus and the second moment of inertia of the model RC pile, respectively) of the model RC pile was 225 ± 8 kNm and 116 ± 38 MNm^2 (mean ± standard deviation), respectively. The coefficient of thermal expansion of the model RC pile along the longitudinal direction was 8.9 ± 1.4 με/˚C (Zhao et al., 2020), which was well within the range for field concrete (6 – 10 με/˚C; Bourne-Webb et al., 2009; Mimouni and Laloui, 2015; Pasten and Santamarina, 2014). The coefficient is assumed to be isotropic. The thermal conductivity of the model RC was measured as 0.73 W/(m.K) (Vitali et al., 2016) and the specific heat capacity was taken as 705 J/(kg.K) (Xu and Chung, 2000).

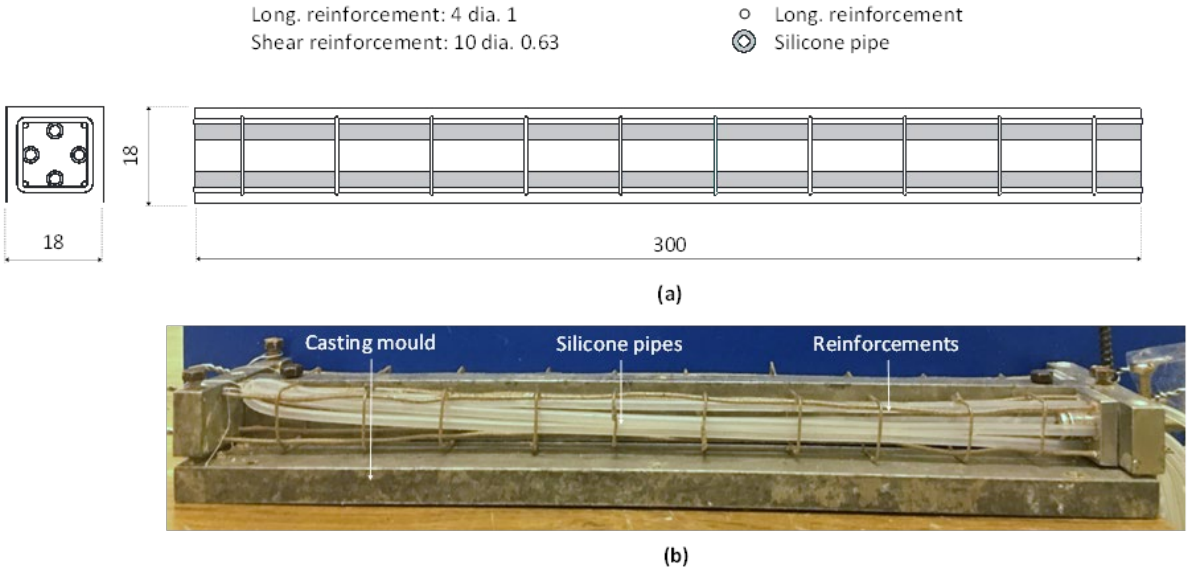

Figure 3. (a) Geometry and reinforcement details of the model RC pile; and (b) arrangement of circulation pipes and steel reinforcement; all units are in millimetre (in model scale)

A temperature-controlled system was built to deliver water of controllable temperature to the model RC pile for simulating heating-cooling cycles during centrifuge flight. The inlet

temperature before entering the model piles was measured by a thermocouple. Three thermocouples were attached to the pile surface at 3.15, 6 and 8.75 m depths below ground level. Each thermocouple has a tip diameter of 1.5 mm. Along the 300-mm-long model pile, the three thermocouples occupied a length of only 4.5 mm. Effects of the thermocouples on the soil–pile interface are thus considered to be negligible. A vertical array of three thermocouples were installed $1D$ away from the pile surface to measure soil temperature changes (Fig. 2(a)).

Test soil and model preparation

The sand used for testing was HST95 Congleton silica sand (Al-Defae et al., 2013; Wang et al. 2018). The average grain size, d_{50} (i.e., particle diameter of 50% passing), was 0.13 mm. For a given pile D of 18 mm (model scale), the ratio, D/d_{50}, was far in excess of 30, meaning that any particle size effect on soil-pile interaction was deemed negligible (Bolton et al., 1999). The ratio was also greater than 92, which suggested that any particle-size effect on the modelling of the thermomechanical behaviour of energy pile could be ignored (Ng et al., 2019). Other mechanical and thermal properties of the sand are summarised in Table 2.

Table 2. Index properties of the HST95 sand used in centrifuge tests and numerical simulations.

Parameter	HST95 silica sand
Mechanical properties	
Specific gravity, G_s	2.63
Maximum void ratio, e_{max}	0.769
Minimum void ratio, e_{min}	0.467
Mean grain diameter, d_{50} (mm)	0.13
Coefficient of uniformity, C_u	1.9
Coefficient of curvature, C_z	1.06
Critical friction angle, ϕ_{crit} (°)	32
Peak friction angle, ϕ_{peak} (°)	39.9 – 45.5
Dilation angle, ψ (°)	9.8 – 16.9
Effective unit weight, γ' (kN/m^3)	10.2
Poisson's ratio	0.32
Saturated density, ρ (kg/m^3)	2041
Thermal properties	
[1]Coefficient of thermal expansion (με/°C)	10
Thermal conductivity (W/(m.K))	0.54 (dry) – 3.03 (saturated)
[2]Specific heat capacity (J/(kg.K))	830 (dry) – 2239 (saturated)

[1]From Rotta Loria et al. (2015a); [2]From Rotta Loria et al. (2015b)

In all three tests, a uniform dry sand bed was produced by air-pluviation within the model box. An average relative density of 67% (i.e., classified as dense; Knappett and Craig, 2019)

was achieved. The model RC pile was installed "wished-in-placed" for an embedded depth of 8.75 m (i.e., ~ 13 times pile width, $13D$) by being hung from suspended wires in the test chamber while the sand was pluviated around it. This essentially modelled a 'bored' pile (Ng et al., 2016a). A free-standing pile length of 1.75 m (i.e., $3D$) was left above the soil surface. The front of the model pile was $8D$ away from the walls of the box. Numerical analyses suggested that any boundary effect due to pile lateral loading was negligible when the pile was $8D$ away from the vertical box boundaries.

Test procedures

In this study, all 1:35 scale models were tested at 22 g. In this way, the effective stresses along any depth of the 1:35 scale piles in the dry physical model would be identical to that of the same physical model tested in fully saturated soil at 35 g. In order to achieve this condition, $\rho_{dry}\, g_{dry}\, z$ should be made equal to $(\rho_{sat} - \rho_w)\, g_{sat}\, z$, where ρ_{dry} and ρ_{sat} are the dry and saturated density of the sand, respectively; g_{dry} and g_{sat} are the g-level for the dry and saturated physical models, respectively; and z is pile depth. For a given sand's relative density (i.e., 67%), g_{dry} needs to be 22. It is vital to highlight that although a g-level of 22 was applied in the centrifuge tests, the scale factor (N) of 35 should be applied to the scaling laws in Table 1 since the problem of interest was scaled down by 35 times, not 22. This modelling technique (i.e., studying 'saturated' soil behaviour using dry soil by manipulating the effective stress regime via the control of g-level) is not uncommon in centrifuge modelling literature (e.g., Li et al., 2010). It was however acknowledged that testing the thermo-active pile in dry sand was a simplification of the problem. Any effects of water on (i) the heat transfer between the pile and the surrounding soil and (ii) the thermomechanical soil-structure interaction were investigated through subsequent numerical sensitivity analyses (reported later).

For the test RP, the motor in the setup shown in Fig. 1 was activated and the pile head was laterally loaded at a controlled rate of 0.03 mm/min (prototype), with continuous measurements of the lateral load mobilised and lateral displacement at the pile head. The lateral push was stopped when the lateral pile displacement reached $0.4D$. At this displacement, prominent tension cracks were developed in the model pile and the pile had reached its limiting lateral capacity and could not take further lateral load. For tests TP21 and TP73, the actuator in the setup shown in Fig. 2 was activated and the mass was released at the same rate of 0.03 mm/min until the desired lateral load was reached. Then, the pile in each test was subjected to three heating-cooling cycles, while the lateral load was maintained. During the heating phases, water of a

controlled temperature of 50 ˚C was delivered to the pile. The duration of the heating phase in the first, second and third cycle was 19, 28 and 12 days, aiming to elevate the pile surface temperature at values typical within the field operation of energy piles (Bourne-Webb et al., 2009). In the subsequent cooling phases, the pile was cooled by circulating 1 ˚C water. The duration of the subsequent pile cooling was 19, 12 and 12 days, providing adequate time for the pile surface temperature to cool to around the ambient conditions. During all heating-cooling cycles, thermally-induced lateral pile displacement was monitored.

Finite-element modelling

The objective of the numerical modelling was to back-analyse the three dry centrifuge tests and conduct a subsequent sensitivity study. The finite-element (FE) platform ABAQUS (2017) was used in this study. When back-analysing tests TP21 and TP73, pile temperature change induced heat conduction to the surrounding soil, following Fourier's Law. Yet, these thermo-mechanical back-analyses were decoupled, meaning that the soil mechanical properties were independent of temperature and any soil volume change would not affect the soil thermal properties. This was deemed acceptable for the modelling of sand and RC, since their thermomechanical properties (Ng et al., 2016c; Takeuchi et al., 1993) and their interface properties (Di Donna et al., 2015; Yavari et al., 2016) were insensitive to temperature changes less than 100 ˚C. Also, recent numerical analyses of thermo-active pile behaviour in sand (Rotta Loria and Laloui, 2016) suggested that using an isothermal mechanical soil model was adequate to capture most of the key sand-pile thermomechanical interaction.

Finite element mesh, boundary and initial conditions

The FE mesh used for the numerical modelling is depicted in Fig. 4. Owing to symmetry, half of the geometry was considered. Prototype dimensions at N = 35 were modelled. As there was (i) no mechanical boundary effects on pile base capacity when the pile toe was more than 3.5D away from the box base (Knappett et al., 2016); and (ii) no thermal boundary effects when the pile centre was more than 8D away from the boundaries based on trial simulations, the modelling domain was smaller than that tested in the centrifuge for saving computational time.

The thermo-active pile was modelled by adapting the method described by Anastasopoulos et al. (2013). The pile was formed from linear beam elements that were circumscribed by hexahedral brick elements. The beam elements were used to act as 'sensors'. The EA and EI of the beam elements are provided by the material properties of the brick elements surrounding the

beams, through provision of equivalent Young's modulus and yield stress to represent the properties of RC piles. So the piles had an axial stiffness provided by the bricks of E_pA_p, but the central beam 'sensors' provided no additional EA (or EI). This method allows direct determination of pile internal forces (via the beam elements), and hence axial response of the pile, while realistically simulating the 3-D geometry of the soil–pile interface. The latter feature was important for allowing heat conduction from the pile to the surrounding soil. Table 3 summarises the input parameters for the 'hybrid' pile modelling.

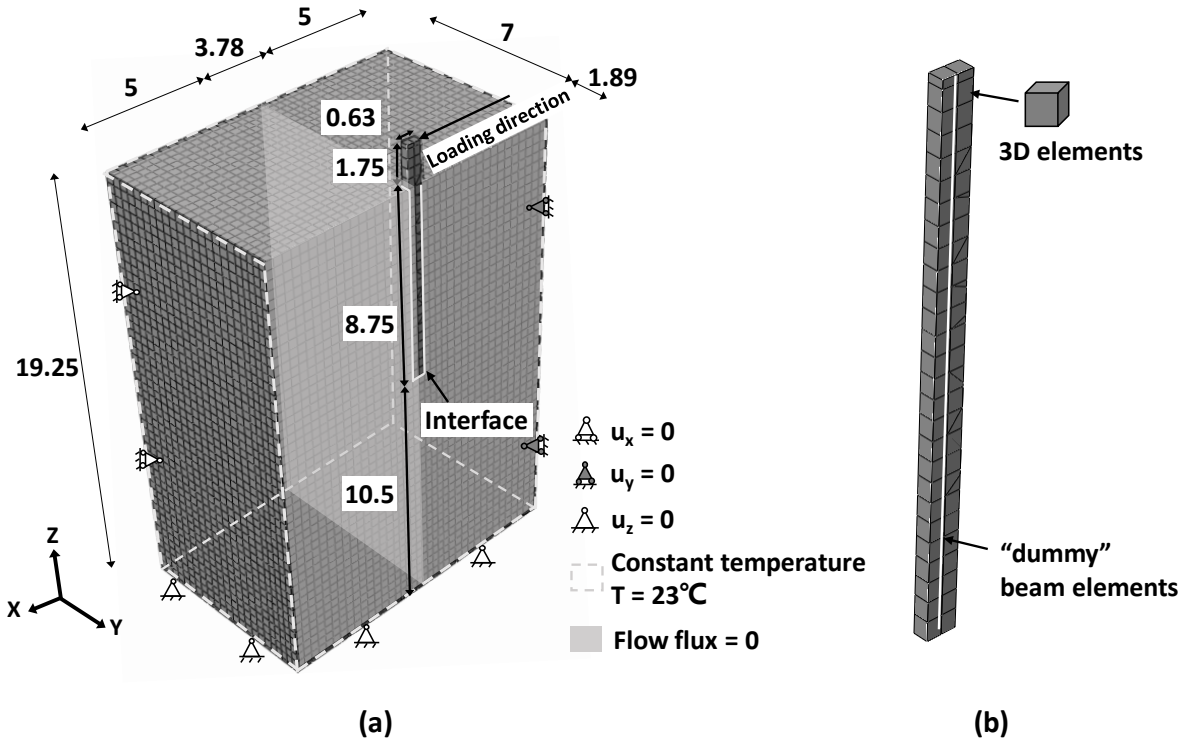

Figure 4. 3D finite element modelling: (a) mesh and boundary conditions; and (b) "hybrid" pile modelling; all dimensions are in m (in prototype scale)

Table 3. A summary of the input parameters for the "hybrid" pile modelling.

Parameter	Brick elements	Beam elements
Mechanical properties		
Bending stiffness, EI (MNm^2)	143	10^{-6}
Poisson's ratio	0.2	0.2
Density, ρ (kg/m^3)	1816	10^{-6}
Thermal properties		
Coefficient of thermal expansion (με/°C)	8.9±1.4	8.9±1.4
Thermal conductivity (W/(m.K))	0.73	0.73
Specific heat capacity (J/(kg.K))	705	705

The soil was made of eight-node hexahedral brick elements based on linear interpolation and normal integration number. The soil-pile interface behaviour was modelled by special contact elements (Anastasopoulos et al., 2011). They allowed for interface shear stress transfer depending on the coefficient of interface friction ($\tan\delta$) via the Coulomb's friction law and permit the pile to be in contact or detach from the surrounding soil. The roughness of the model concrete was 5.09 ± 0.93 μm (measured by a surface roughness tester; SJ 201 Mitutoyo) corresponding to a value of 0.6 for $\tan\delta$, following an empirical curve of soil-pile interface friction and roughness normalised by d_{50} in Knappett and Craig (2019).

The bottom boundary of the FE model was constrained in the vertical direction, while only vertical displacement was permitted along the side boundaries. The soil surface was free to move in any direction. Regarding the thermal boundary conditions, except the surface of symmetry and the soil surface, thermal constraint of 23 ºC (ambient in the centrifuge) was applied on the other external surfaces of the mesh, permitting heat to flow through these surfaces. Along the surface of symmetry and the soil surface, the heat flux was imposed to be null. When modelling the heating-cooling cycles in tests TP21 and TP73, the variation of the input pile surface temperature with time was taken to be the average value between 3.15 and 6 m depths and applied along the entire pile volume. Detailed pipe-mortar (i.e., model RC)-soil heat transfer process was not explicitly modelled, in order to avoid the large contrast of mesh between the pipe and the pile elements, which would introduce numerical instabilities to solve this complex thermomechanical lateral soil-pile interaction problem. Indeed, the field experiments carried out by Faizal et al. (2019) have shown that the radial distribution of temperature (hence thermally-induced axial strain) was rather uniform across the pile cross-section during heating and cooling cycles. Any temperature gradient developed within the internal structure of the RC energy pile may be reasonably neglected. The initial stresses within the pile and the soil in the numerical model were established by the application of self-weight with a coefficient of earth pressure at rest (K_0) of 0.47. The initial temperature of the soil, pile and the pile-soil interface were set to be the average ambient temperature of 23 ˚C recorded from the centrifuge tests.

Constitutive models and material properties

Two constitutive soil models of varying degree of complexity were considered. The first model was the linear-elastic (LE) Mohr Coulomb (MC) model considering stiffness linearised from the nonlinear small-strain stiffness behaviour consistent with the shear strains developed during the initial lateral loading using an iterative procedure (denoted as LEMC small model). The

second model was the MC softening model, which added post-peak softening responses at large strain to the LEMC small model. Both the LEMC small and MC softening models have been validated against drained triaxial compression tests and a set of centrifuge tests on non-thermal piles by Zhao et al. (2021).

In both models, the elastic behaviour was characterised by v and E (= G/(2(1+ v)), where G was the elastic shear modulus and v was the Poisson's ratio. In order to capture the stress-dependency on stiffness of the sand, firstly, the FE mesh representing the soil was split into nine horizontal layers. The initial shear modulus (G_0) of each layer with an average confining pressure was calibrated against existing triaxial test data (D_r = 70%, p'_0 between 20 to 60 kPa) of the sand. Strain-dependency on G was also considered. Using the initial G_0 distribution, the pile was subjected to the lateral load (i.e., either at 21% or 73% of the peak lateral load) for determining the mobilized engineering shear strain (γ) profile of the soil elements immediately in front of the pile at a range of depths (i.e., in the passive zone) in each layer. These values were subsequently mapped to the G- γ curves reported by Ishibashi and Zhang (1993) for deducing a new (mobilised) G profile. The G profile was then updated in the model as a new initial parameter distribution and the lateral load stage re-run. These steps were repeated until the change of γ between each successive steps was less than 0.001%. The resulting profiles of mobilised γ and G for the piles subjected to 21% and 73% of the peak lateral load are shown in Fig. 5. The method adopted to take into account the nonlinear strain dependency of the mobilised stiffness is a pragmatic approximation to reality, when using a relatively simple and widely available constitutive soil model that uses linear elasticity such as the MC model.

Both soil models followed the Mohr-Coulomb failure criterion. For the LEMC small model, the effects of confining pressure on friction angle and dilation angle were considered using a non-associative model. In each soil layer, the friction and dilation angles at the corresponding effective confining pressures were determined by the empirical equation proposed by Bolton (1986). For the MC softening model, the critical-state friction angle ($\emptyset_{crit}$ = 32°) and dilation angle (ψ = 1°) were input. To capture the peak and post-peak softening behaviour in this soil model, the plastic potential surface was additionally defined by an apparent cohesion stress-plastic shear strain (c'- γ_p) relationship. c' was defined by a hyperbolic function (Menétrey and Willam, 1995) of mean stress (p') and von Mises deviator stress (q). Both c' and γ_p were calibrated by best-fitting drained triaxial compression tests conducted at p'_0 = 20 to 60 kPa (see the case of 60 kPa as an example in Fig. 6 after Sharif et al., 2019). Soil parameters for the p'_0 of 20, 40 and 60 kPa were input into the 1st – 2nd, 3rd and 4th – 9th layers, respectively.

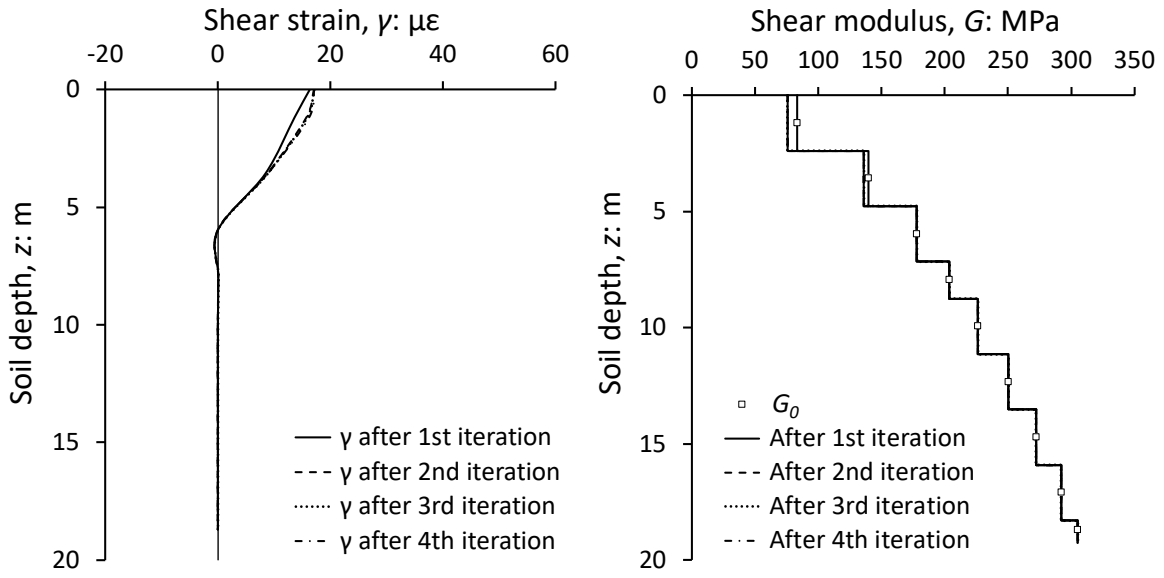

(a)

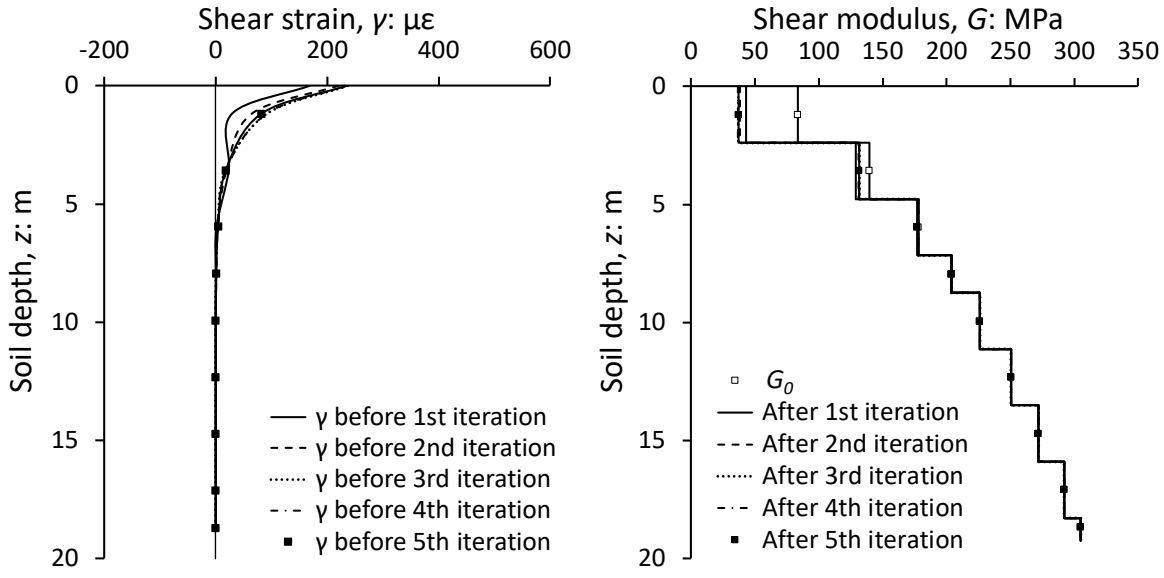

(b)

Figure 5. Mobilised shear strain (left) and shear modulus (right) of the sand when the pile is subjected to (a) 21% (TP21) and (b) 73% (TP73) of the ultimate pile lateral capacity

In all models, an effective unit weight of 10.2 kN/m^3 corresponding to the sand D_r of 67% was applied, so that the soil considered in the model was apparently 'fully-saturated'. Because of the limitation of the Finite Element solver used, the creep module cannot be activated with the soil model used and hence any mechanical creep of soil could not be considered in the modelling conducted.

For the thermal properties, the empirical equation derived for silica sand by Chen (2008) was used to determine the thermal conductivity of the dry sand under different values of void ratio at different soil depths for input into each soil layer. Other thermal properties, including the specific heat capacity and thermal expansion coefficient, are summarised in Table 2.

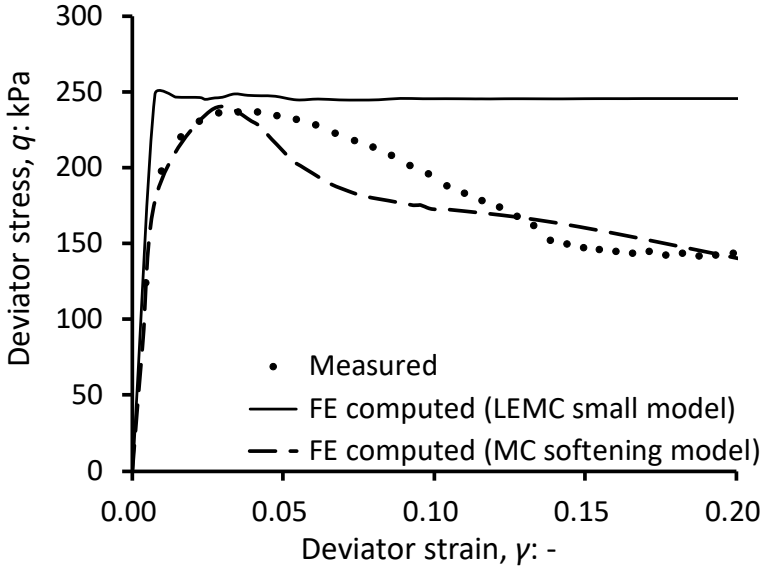

Figure 6. Calibration of a deviatoric stress-shear strain curve of the dense sand (D_r = 70%) at p'_0 = 60 kPa (triaxial data from Sharif et al., 2019), as a typical example

For the pile, an elasto-plastic model was used to capture the nonlinear behaviour of the RC. The elastic part was characterised by the pile bending stiffness and ν (= 0.2 for mortar; Corinaldesi, 2009). The plastic response of the pile was defined by a plastic flexural stress-strain relationship derived from the FPB tests (Fig. 7(a)). By applying this pile constitutive model to simulate the FPB test, both the computed initial pile bending stiffness (143 MNm^2) and the ultimate bending moment (238 kNm) matched the respective measured values (Fig. 7(b)). The RC pile obeyed thermal elasticity. To allow for representative heat conduction from the pile to the surrounding soil through the soil-pile interface, the thermal conductivity of the interface was set to a large value (i.e., 400 W/(m.K); more than 100 times of the thermal conductivity of the saturated sand; refer to Table 2) to avoid additional thermal resistance from the interface. Prior mesh refinement analysis shows that the aspect ratio of FE mesh adopted (i.e., 1.3) did not introduce any mesh size effect to the calculation accuracy.

To capture the effects of mechanical creep of the model RC pile, a power-law model in the time-hardening form was adopted (ABAQUS, 2017):

$$\dot{\varepsilon} = Aq^n t^m \tag{3}$$

where $\dot{\varepsilon}$ is the creep strain rate; q is the uniaxial deviatoric stress (MPa); t is the creep duration (s); and A, n and m are the material parameters of the mortar. Because of the lack of creep data of reinforced mortar, A, n and m, in this study are treated as best-fitting parameters to match the thermally-induced pile head displacement. They are taken as 5.03 x 10^{-5} (in the unit of $s^{0.5}$), 0 and -0.5, respectively.

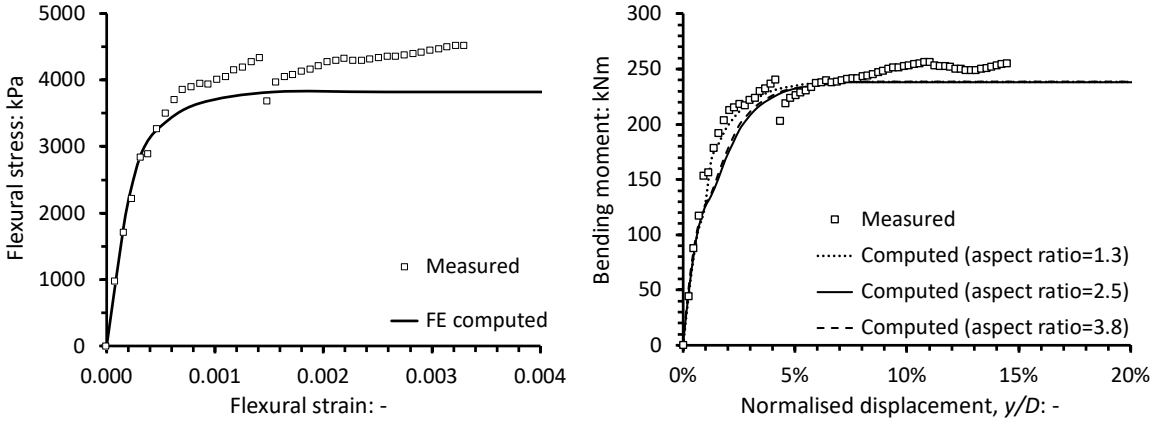

(a) (b)

Figure 7. Comparisons between measured and FE-computed (a) flexural stress-strain curve and (b) moment-curvature curve of the model RC pile

Interpretation of measured and computed results

Lateral load-displacement curves

Figure 8(a) shows the pile head horizontal load-displacement curve obtained from the tests RP and TP21. The soil-pile flexural behaviour was approximately linear initially, before reaching a yield load of approximately 119 kN at a displacement of $0.1D$. The soil-pile system tested in TP73 was stiffer than that in test RP, likely due to the effects of material variabilities and workmanship during the production of the model RC piles (Vitali et al., 2016; Knappett, 2018). For TP21, the pile initially showed similar stiffness to RP, but beyond 0.1% displacement was stiffer and then exhibited a significant increase in displacement at near constant load (inset, Fig. 8(a)). This is thought to be due to the onset of first cracking in this specific model pile, as some model-scale beams fabricated from the model RC have been observed to exhibit such behaviour in four-point bending tests at $0.25M_{ult} < M < 0.4M_{ult}$ (where M_{ult} is the ultimate moment capacity; Loli, 2015). Moreover, although all the model piles were ready for testing after 28-day curing, the model piles used in TP21 and TP73 were tested months after those used in RP. Additional material hardening with time might partly explain the stiffer responses of the 'older' model piles in the thermal tests. Pile head displacements predicted by the two

soil models were close to those measured in test TP21. As the load level was low, there was limited plastic soil strain mobilised such that the two models operated with the same elastic model. Figure 8(b) compares the measured and predicted results for tests RP and TP73. Similar observations with the previous case were found. At higher mobilised load, there was more extensive plastic soil strain such that the models deviated from each other in their predictions.

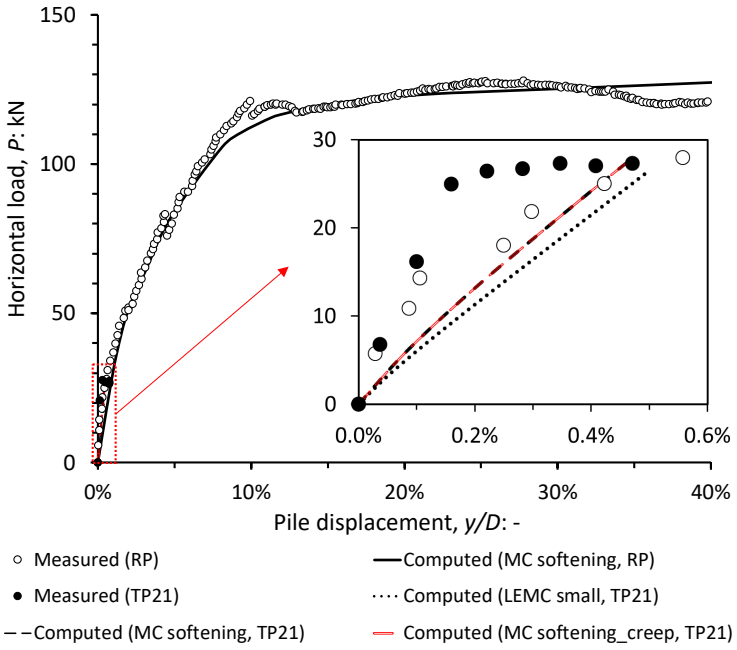

(a)

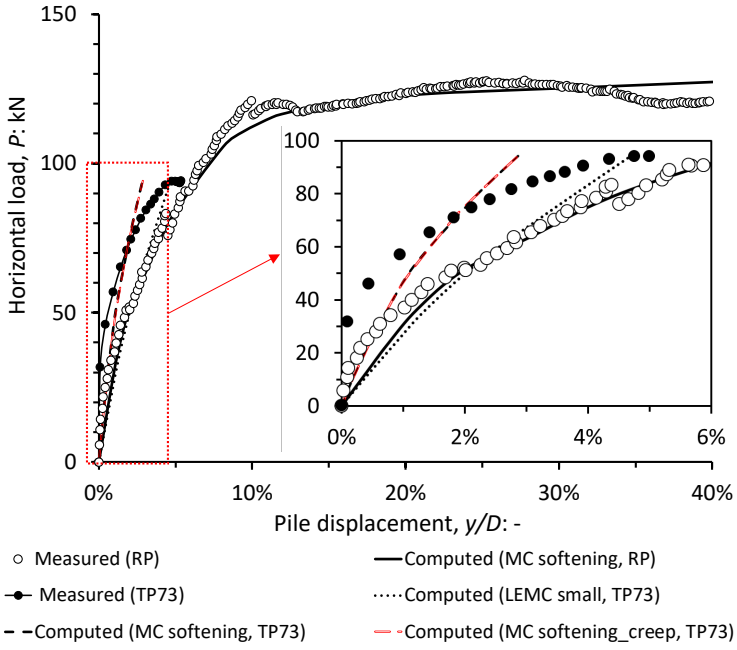

(b)

Figure 8. Measured and FE-computed horizontal load-displacement curves: (a) TP21, (b) TP73

Temperature responses

Figure 9 shows the variations of the temperature measured at the pile surface and in the soil at 1D radially away from the pile surface, at 3.15 and 6 m depths with time. Although water of 50 ˚C was circulated to the model pile in both tests, a portion of the heat energy was absorbed in the mortar and the reinforcement of the model RC, mimicking what typically occurs in thermo-active piles in the field (Loveridge and Powrie, 2014; Poppei et al., 2008). On average, the increase in pile surface temperature was 5 ˚C. In both tests, the increase in pile surface temperature during all heating stages was always higher than that in soil because the dry soil had lower thermal conductivity (compared to the model RC) and this caused thermal resistance as the heat conducted radially. During each cooling cycle, again due to the thermal mass of the various components within the model RC, the pile surface temperature did not drop to the target value of 1 ˚C. Instead, both the pile surface and soil temperature returned to the ambient. The pile surface temperature induced in the case of TP21 was higher than that in TP73, probably because of the variabilities of the thermal conductivity of the model RC (Zhao et al., 2020).

In general, the FE-predicted soil temperatures, at both 3.15 and 6 m depths, matched well with the measurements in both tests TP21 and TP73. This implied that ignoring any change of the sand thermal properties due to soil volumetric change (upon mechanical and/or thermal loading) introduced only a minimal effect on the soil temperature prediction.

Thermally-induced horizontal pile head displacement

Figure 10 compares the measured and computed thermally-induced pile head displacement during the three repeated heating-cooling cycles. At 21% of the ultimate lateral capacity (i.e., test TP21; Fig. 10(a)), the pile head displacement was 0.87%D. The measurements showed that the thermally-induced pile head displacement increased steadily during the three heating-cooling cycles. At higher mobilised horizontal load (i.e., test TP73; Fig. 10(b)), the pile head displacement was higher (i.e., 6.55% D). The thermally-induced pile head showed a clear movement towards the loading direction by up to 0.75%D during the first heating cycle. During the subsequent cooling cycle, the pile head displacement remained approximately unchanged. In the second and third heating-cooling cycles, the same phenomena repeated, yet the magnitude of pile head displacement was less than that during the first cycle. The pile head displacement therefore accumulated and there was always a net pile head movement in the direction of the maintained horizontal load after each cycle (i.e., thermal ratcheting).

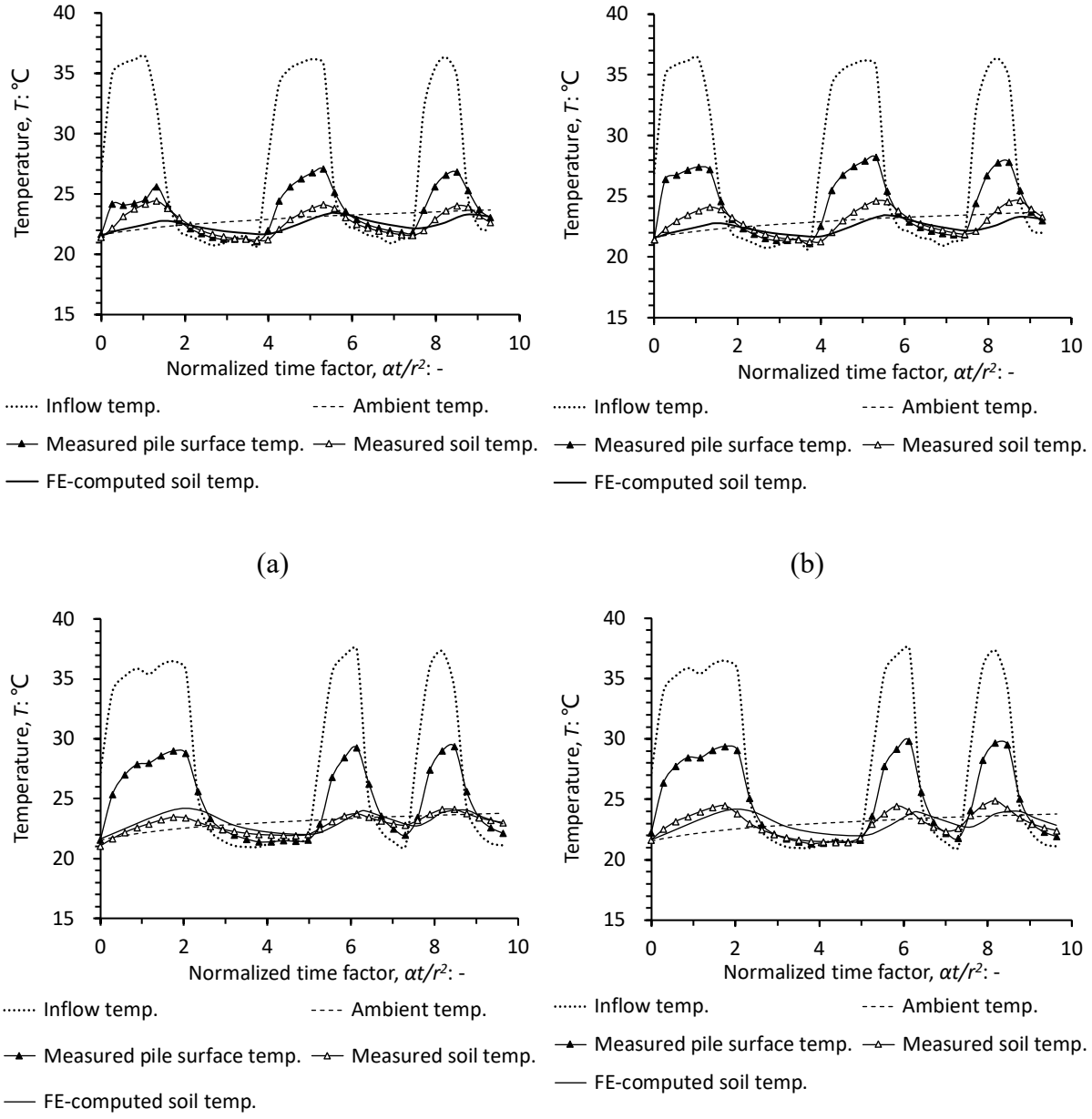

Figure 9. Comparisons of measured and FE-computed temperature variations at the pile surface and soil (1D away from the pile surface) with time (a) at 3.15 m depth and (b) 6 m depth for test TP21; (c) at 3.15 m depth and (d) 6 m depth for test TP73

When not considering pile mechanical creep, the pile head ratcheting was reasonably captured by the FE-prediction, especially during the first heating-cooling cycle. Discrepancies, however, was more prominent during the second and third cycles, where the pile displacement was underestimated by the FE-prediction. When creep was considered, more displacement was predicted, as expected, and this led to a better prediction in both the second and third cycles. There was still a difference in the third cycle, which may be attributed to two main reasons.

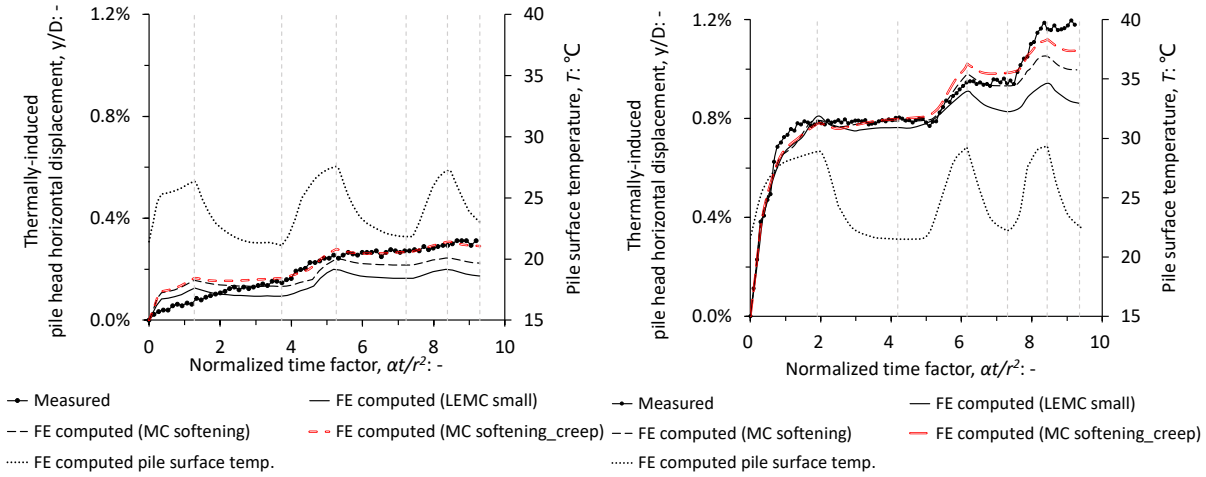

(a) (b)

Figure 10. Measured and FE-computed thermally-induced pile head lateral displacement for tests (a) TP21; and (b) TP73

First of all, soil creeping was not considered in the simulations because the constitutive model adopted did not permit simultaneous use of the user-defined MC softening model and any available creep model. Nguyen et al. (2017) who tested an axially-loaded aluminium energy pile in dry silica sand has demonstrated an increase in pile displacement under a constant load at a constant room temperature due to soil creep. The creep coefficient (C_α) of dry silica sand (at a void ratio of 0.61) can be estimated as 0.0878 mm/hr (Duttine et al., 2009). Hence, after five hours (model scale) of maintained load for the three heating-cooling cycles in both centrifuge tests, the total creep displacement from the sand may be estimated to be 0.43 mm (or 0.07%D). This is close to the difference between the measurements and FE simulations in the third cycle. This suggests that an important piece of future work will be to conduct additional study to fully parameterise and comparatively evaluate different thermo-elasto-plastic constitutive models incorporating mechanical and thermal creep. The second reason is the uncertainty associated with the scaling laws of mechanically- and thermally-induced creep displacement (Garnier et al., 2007). Due to the lack of understanding in the centrifuge modelling literature, it is unclear how the mechanically- and thermally-induced creep displacement of soil measured in a centrifuge test should be scaled to prototype for comparison with the FE prediction. Further study of the scaling of creep (both mechanical and thermal) is needed in the future.

In general, the predictions made by the MC softening model were significantly better in this regard compared to the LEMC small model. This implied that in addition to capturing the

small-strain nonlinearity, it was important to also consider large-strain post-peak soil softening (Fig. 6) when predicting the thermally-induced horizontal pile head displacement.

Discussion

Upon pile heating (Figs 11(a) and (d)), the top 4.8 m of the pile displaced in the direction of the maintained horizontal load (Figs 11(b) and (e)). The pile displacement was smaller at deeper depths because of higher soil subgrade reaction modulus. Despite uniform pile heating, the pile axial tensile strain developed was non-uniform (Figs 11(c) and (f)). Greater strains were found at 0 to 3 m soil depths, where substantial pile movement and bending occurred (see later). These axial strains were the results of three mechanisms (i) pile thermal strain upon expansion, (ii) pile mechanical strain due to the axial component of the horizontal load and (iii) pile creep strain due to the maintained load. The pile axial strain reduced slightly with soil depth (i.e., less tensile) because of the increased mechanical restraint by the surrounding soil with depth. The strain developed in the test TP73 (Fig. 11(g)) was higher than that in TP21 (Fig. 11(c)) because the pile in the former case was subjected to slightly higher temperature increase (mechanism (i); refer to Fig. 9) and higher horizontal load applied (mechanism (ii)).

During heating, pile lateral expansion induced horizontal stress and strain to the soil element in the vicinity of the pile, while pile axial expansion induced shearing at the soil-pile interface. Due to soil dilation, the latter action also introduced some additional horizontal strain, being more significant near the pile head because of lower confinement. These combined actions explain the increase and decrease in the deviator strains upon pile heating and cooling, respectively (Figs 12(a) and (b), for the soil element in front of the pile at 1.19 m soil depth where the pile bending moment peaked).

Upon pile cooling, the pile contracted and rebounded but it did not return to the original position (Figs 11(b) and (e)). The pile contraction introduced compressive axial strain increments, making them much less tensile along the pile length at the end of cooling (Figs 11(c) and (f)). Compared with the axial strain produced by the mechanical loading (see the solid line in Figs 11(c) and (f)), residual axial tensile strains were resulted after a heating-cooling cycle. This is partly because of the pile creep and partly due to the accumulation of soil plastic strain after a cycle of lateral loading (caused by pile thermal expansion upon heating) and unloading (caused by pile contraction upon cooling). Unloading accompanied by the pile thermal contraction caused reductions of the deviator strain (Figs 12(a) and (b)).

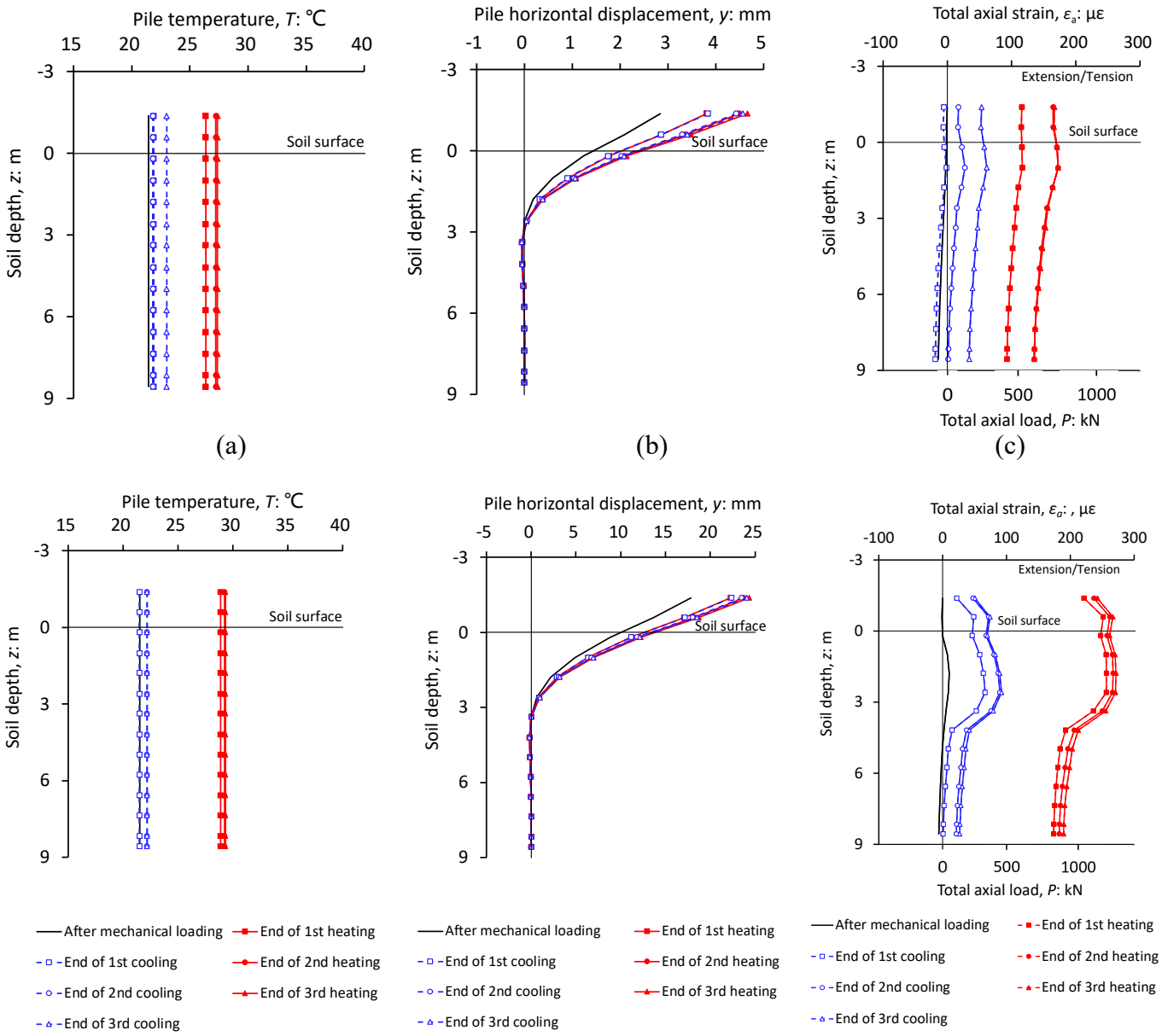

Figure 11. Profiles of (a, d) pile surface temperature change; (b, e) pile horizontal displacement; (c, f) pile axial strain and pile axial load for tests TP21 ((a), (b), (c)) and TP73 ((d), (e), (f)). Note that the range of the bottom x-axis for Figs 11(c) and (f) is from -432 to 1296 kN.

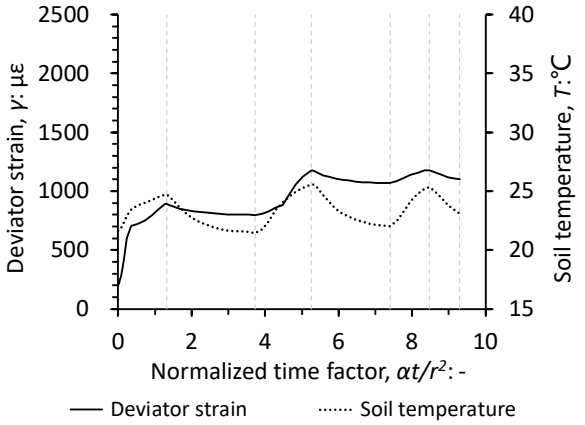

529

530 (a)

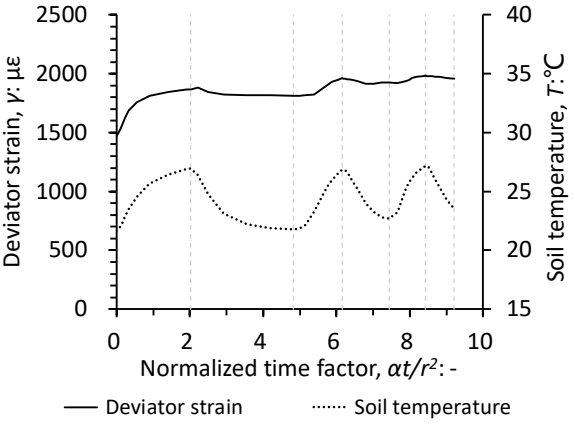

(b)

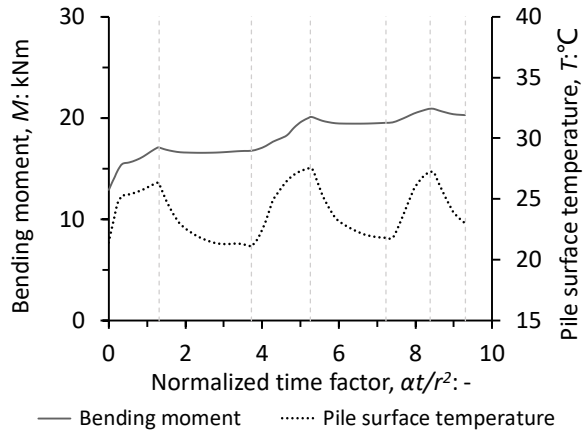

532 (c)

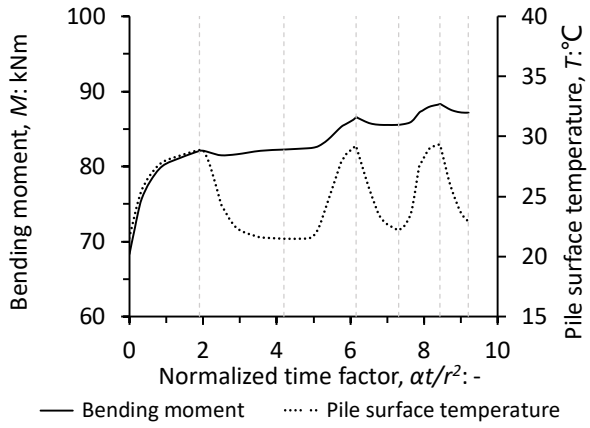

(d)

536

537 Similar mechanisms occurred in the 2nd and 3rd heating-cooling cycles (Fig. 11). The load-
538 ing-unloading cycles arising from the pile lateral thermal expansion and contraction as well as
539 pile creep were responsible for further yielding of the soil in the vicinity of the pile. This soil
540 yielding translated to further accumulation of deviator strain (Figs 12(a) and (b)). Compared
541 with the 1st heating-cooling cycle, the net increases in the deviator strain after the 2nd and 3rd
542 cycles were smaller. In effect, the three heating-cooling cycles resulted in the application of
543 cyclic mechanical horizontal and shear load to the soil elements in the vicinity of the pile,
544 superimposed on that present due to the maintained lateral load. This repeated mechanical
545 shearing yielded the soil and led to an accumulation of deviator strain, with the magnitude of
546 strain increase reducing with increasing cycle number. This is consistent with the cyclically-

increasing bending deformations within the pile (Figs 12 (b) and (e)). Due to the practical difficulties of installing strain gauges within the small-scale model RC piles in the present study, thermally-induced pile stress and strain could not be measured. The FE predictions thus explain the soil-pile interaction qualitatively.

Figure 13 shows the computed mobilised pile bending moment during the three cycles of thermal loading for test TP73. Evidently, the first heating induced a significant increase in pile moment in the top 4.8 m. While the pile moment accumulated in each cycle, the depth of the moment peaks was unchanged. Also, the three heating-cooling cycles did not adversely affect the structural integrity of the RC pile since the final mobilised pile bending moments remained far from the ultimate value of 225 kNm.

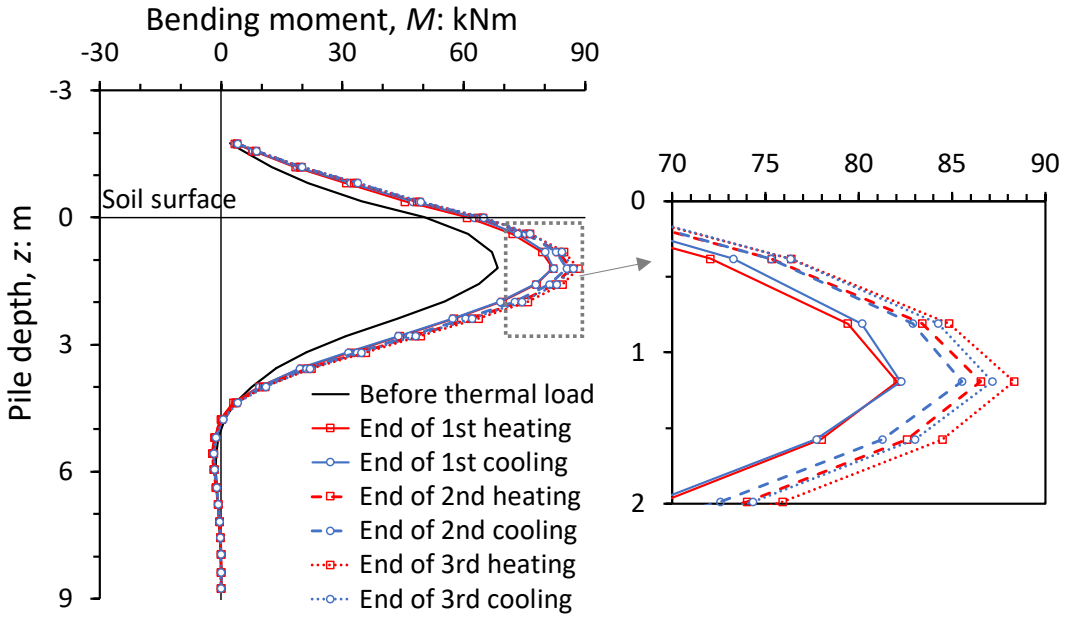

Dry sand was considered in both the centrifuge tests. Although the effective stress regime in these dry sand tests was equivalent to the fully saturated prototype, the effect of water on the thermal conductivity of the sand could not be considered. To investigate this effect on the thermomechanical sand-pile interaction and the pile ratcheting behaviour, a sensitivity analysis was conducted based on test TP73. In this analysis, the sand thermal properties including the specific thermal capacity and thermal conductivity of the dry sand as tested in the centrifuge (c_{dry} of 830 J/(kg.K); λ_{dry} of 0.54 W/(m.K)) were replaced by those of saturated sand (c_{sat} of 2239 J/(kg.K); λ_{sat} of 3.03 W/(m.K)) (see Table 2), consistent with the effective stress conditions that were modelled. Similarly, the thermal conductivity of the soil-pile interface was set

570 at a large value of 400 W/(m.K)). The MC softening model, which was found to give the best
571 predictions of the centrifuge data, was used. The computed results showed that the value of the
572 thermal conductivity used had a negligible effect (between the dry and saturated values) on the
573 sand-pile interaction including the pile ratcheting behaviour and the pile bending moments.
574 When a higher thermal conductivity was used, for a given period of heating (or cooling) dura-
575 tion, a greater volume of sand was heated (or cooled), meaning that more sand was subjected
576 to thermal expansion (or contraction). However, for the range of thermal conductivity (0.54 to
577 3.03 W/(m.K)) and the coefficient of thermal expansion of the sand (10 $\mu\varepsilon/^{\circ}C$) considered, the
578 difference in thermo-elastic strain was too small to introduce noticeable effects on the pile head
579 ratcheting and induced bending moments. Hence, the dry sand centrifuge tests were representa-
580 tive of a fully saturated prototype.
581
582 **Summary and conclusions**
583 This study used a combination of centrifuge and three-dimensional numerical modelling tech-
584 niques to investigate the thermally-induced ratcheting behaviour of a laterally-load thermo-
585 active pile in sand. A newly-developed model reinforced concrete (RC) was used in the centri-
586 fuge tests to realistically mimic prototype nonlinear thermomechanical soil-pile interaction.
587 Finite Element analysis considered nonlinear behaviour of the model RC thermo-active pile
588 including mechanaicl creep as well as small-strain nonlinearity and large-strain, post-peak soft-
589 tening behaviour within the soil. Based on the measured and computed results, it was evident
590 that applying cyclic thermal loading introduced net increases in the lateral pile head displace-
591 ment and mobilisation of pile bending moment, especially when the pile was subjected to a
592 high maintained lateral load. At a working lateral load of 73% of the maximum lateral load,
593 the additional moment caused by repeated pile thermal loadings, however, did not make the
594 pile yield or fail. The underlying mechanism behind the observed pile ratcheting phenomenon
595 was attributed to the accumulation of plastic strains within the surrounding soil as a result of
596 the cyclic mechanical loading induced by pile horizontal expansion upon heating and unloading
597 by pile contraction upon cooling, soil dilation upon soil-pile interface shearing and creep.
598 Sensitivity analyses showed that it was important to capture both the small-strain nonlin-
599 earity and the large-strain, post-peak softening behaviour of sand for more accurate prediction
600 of thermally-induced pile ratcheting behaviour in sand. Ignoring the softening behaviour un-
601 derestimated the magnitude of the accumulated pile head lateral displacement significantly.
602 The analyses also showed that (i) ignoring the thermoelastic response of sand and (ii) using
603 either the values of thermal conductivity for dry or fully saturated sand had minimal effects on

the magnitude of thermally-induced pile head displacements and bending moments. These results implied that numerical models can improve the prediction of thermally-induced horizontal pile head ratcheting in sand as long as the model can capture pile thermo-elastic volume change and post-peak strain-softening behaviour of the sand. To further improve the predictability of the numerical modelling, further work is needed to develop more advanced thermomechanical constitutive models of soil and reinforced concrete that can capture both mechanical and thermal creep in all model materials.

Data availability statement

Some or all data used are available from the corresponding author by request.

Acknowledgements

The authors acknowledge the funding provided by the National Natural Science Foundation of China (NSFC) including the Basic Science Center Program for Multiphase Media Evolution in Hypergravity of the NSFC (no. 51988101), the Excellent Youth Scientist Scheme (H. K. & Macau) (project no. 51922112) and the studentship provided by the Chinese Scholarship Council. The authors also acknowledge the help provided by Prof. Ioannis Anastasopoulos of ETH, Zurich, for setting up the finite-element numerical model at the initial stage of the project.

References

Abaqus. (2017). ABAQUS V.6.14 user's manual, Providence, R.I.

Al-Defae, A. H., Caucis, K., and Knappett, J. A. (2013). Aftershocks and the whole-life performance of granular slopes. *Géotechnique* **63**, No. 14, 1230–1244.

Anastasopoulos, I., Gelagoti, F., Kourkoulis, R. and Gazetas, G. (2011). Simplified constitutive model for simulation of cyclic response of shallow foundations: validation against laboratory tests. *J. Geotech. Geoenviron. Eng.* **137**, No. 12, 1154-1168.

Anastasopoulos, I., Kourkoulis, R., Gazetas, G. and Tsatsis, A. (2013). Interaction of piled foundation with a rupturing normal fault. *Géotechnique* **63**, No. 12, 1042-1059.

Bolton, M. D. (1986). The strength and dilatancy of sands. *Géotechnique* **36**, No. 1, 65-78.

Bolton, M. D., Gui, M. W., Garnier, J., Corte, J. F., Bagge, G., Laue, J. and Renzi, R. (1999). Centrifuge cone penetration tests in sand. *Géotechnique* **49**, No. 4, 543-552.

Bourne-Webb, P. J., Amatya, B., Soga, K., Amis, T., Davidson, C. and Payne, P. (2009). Energy pile test at Lambeth College, London: geotechnical and thermodynamic aspects of pile response to heat cycles. *Géotechnique* **59**, No. 3, 237-248.

638 Brandl, H. (2006). Energy foundations and other thermo-active ground structures. *Géotech-*
639 *nique* **56**, No. 2, 81-122.
640 Brennan, A. J., Knappett, J. A., Bertalot, D., Loli, M., Anastasopoulos, I. and Brown, M. J.
641 (2014). Dynamic centrifuge modelling facilities at the University of Dundee and their ap-
642 plication to studying seismic case histories. *Proc. Int. J. Phy. Modell. In Geotech.,* 227-233,
643 UK.
644 Chen, S. X. (2008). Thermal conductivity of sands. *Heat Mass Transfer* **44**, No. 10, 1241-1246.
645 Corinaldesi, V. (2009). Mechanical behavior of masonry assemblages manufactured with
646 recycled-aggregate mortars. *Cem. Concr. Compos.* **31**, No. 7, 505-510.
647 Di Donna, A., Ferrari, A. and Laloui, L. (2015). Experimental investigations of the soil-con-
648 crete interface: physical mechanisms, cyclic mobilisation and behaviour at different temper-
649 atures. *Can. Geotech. J.* **53**, No. 4, 659-672.
650 Di Donna, A., Rotta Loria, A. F. and Laloui, L. (2016). Numerical study of the response of a
651 group of thermo-active piles under different combinations of thermo-mechanical loads.
652 *Comput. Geotech.* **72**, 126-142.
653 Duttine, A., Tatsuoka, F., Lee, J. and Kongkitkul, W. (2009). Viscous property of Toyoura
654 sand over a wide range of shear deformation rate and its model simulation. *Soils Found.* **49**,
655 No. 2, 231-247.
656 Faizal, M., Bouazza, A., McCartney, J. S., and Haberfield, C. (2019). Axial and radial thermal
657 responses of energy pile under six storey residential building. *Can. Geotech. J.* **56**, No. 7,
658 1019 – 1033.
659 Garnier, J., Gaudin, C., Springman, S. M., Culligan, P. J., Goodings, D., Konig, D., Kutter, B.,
660 Phillips, R., Randolph, M. F., and Thorel, L. (2007). Catalogue of scaling laws and simili-
661 tude questions in geotechnical centrifuge modelling. *Proc. Int. J. Phy. Modell. In Geotech.*
662 **7**, No. 3, 1 – 23.
663 Gawecka, K. A., Taborda, D. M. G., Potts, D. M., Cui, W., Zdravkovic, L., Kasri, M. S. H.
664 (2017). Numerical modelling of thermo-active piles in London Clay. *Proc. ICE, Geotech.*
665 *Eng.* **170**, No. 3, 201 – 219.
666 Goode III, J. C. and McCartney, J. S. (2015). Centrifuge modeling of end-restraint effects in
667 energy foundations. *J. Geotech. Geoenviron. Eng.* **141**, No. 8, p.04015034.
668 Iai, S., T. Tobita, and T. Nakahara. (2005). Generalised scaling relations for dynamic centrifuge
669 tests., *Géotechnique* **55**, No. 5, 355–362.
670 Ishibashi, I., and Zhang, X. (1993). Unified dynamic shear moduli and damping ratios of sand
671 and clay. *Soils Found.* **33**, No. 1, 182-191.

672 Knappett, J. A., Brown, M. J., Shields, L., Al-Defae, A. H. and Loli, M. (2018). Variability of
673 small scale model reinforced concrete and implications for geotechnical centrifuge testing.
674 *Proc. Int. J. Phy. Modell. In Geotech.* **1**, 241-246, UK.
675 Knappett, J. A., and Craig, R. F. (2019). *Craig's soil mechanics,* 9th Ed., London, UK: Spon
676 Press.
677 Knappett, J. A., Caucis, K., Brown, M. J., Jeffrey, J. R. and Ball, J. D. (2016). CHD pile
678 performance: part II–numerical modelling. *Proc. Inst. Civil Eng. – Geotech. Eng.* **169**, No.
679 5, 436-454.
680 Knappett, J. A., Reid, C., Kinmond S., and O'Reilly, K. (2011). Small-Scale Modeling of Re-
681 inforced Concrete Structural Elements for Use in a Geotechnical Centrifuge. *J. Struct. Eng.*
682 **137**, No. 11, 1263-1271.
683 Loli, M.D. (2015). Non-linear seismic interaction between soil and slender structure. PhD The-
684 sis, National Technical University of Athens, Athens, Greece.
685 Loveridge, F. A. and Powrie, W. (2013). Pile heat exchangers: thermal behaviour and interac-
686 tions. *Proc. ICE-Geotech. Eng.* **166**, No. 2, 178-196.
687 Loveridge, F., and Powrie, W. (2014). 2D thermal resistance of pile heat exchangers. *Geother-*
688 *mics* **50,** 122–135.
689 Li, Z., Haigh, S. K. and Bolton, M. D. (2010). Centrifuge modelling of mono-pile under cyclic
690 lateral loads. *Proc. Int. J. Phy. Modell. In Geotech.* **2**, 965-970, Switzerland.
691 Menétrey, P. and Willam, K.J. (1995). Triaxial Failure Criterion for Concrete and its General-
692 ization. *ACI Structural Journal* **92**, No. 3, 311-318.
693 Mimouni, T. and Laloui, L. (2015). Behaviour of a group of energy piles. *Can. Geotech. J.* **52**,
694 No. 12, 1913-1929.
695 Ng, C. W. W., Gunawan, A., Shi, C., Ma, Q. J. and Liu, H. L. (2016a). Centrifuge modelling
696 of displacement and replacement energy piles constructed in saturated sand: a comparative
697 study. *Geotechnique Lett.* **6**, No. 1 , 1-5.
698 Ng, C. W. W., Ma, Q. J. and Gunawan, A. (2016b). Horizontal stress change of thermo-active
699 piles subjected to thermal cycles in sand. *Comput. Geotech.* **78**, 54-61.
700 Ng, C. W. W., Shi, C., Gunawan, A., and Laloui, L. (2014). Centrifuge modelling of thermo-
701 active piles subjected to heating and cooling cycles in clay. *Geotechnique Lett.* **4**, No. 4,
702 310-316.
703 Ng, C. W. W, Shi, C., Gunawan, A., Laloui, L., Liu, H. L. (2015). Centrifuge modelling of
704 heating effects on energy pile performance in saturated sand. *Can. Geotech. J.* **52**, No. 8, 1-
705 13.

706 Ng, C. W. W., Wang, S. and Zhou, C. (2016c). Volume change behaviour of saturated sand
707 under thermal cycles. *Geotechnique Lett.* **6**, No. 2, 124-131.
708 Ng, C. W. W., Zhang, C., Farivar, A. and Gomaa, S. M. M. H., (2019). Scaling effects on the
709 centrifuge modelling of energy piles in saturated sand. *Géotechnique Letters* **10**, No. 1, 1-6.
710 Nguyen, V. T., Tang, A. M. and Pereira, J. M. (2017). Long-term thermo-mechanical behavior
711 of energy pile in dry sand. *Acta Geotechnica* **12**, No. 4, 729-737.
712 Pasten, C. and Santamarina, J. C. (2014). Thermally induced long-term displacement of ther-
713 moactive piles. *J. Geotech. Geoenviron. Eng.* **140**, No. 5, p.06014003.
714 Poppei, J., Schwarz, R., Peron, H., Silvani, G., Steinmann, G., Laloui, L., Wagner, R.,
715 Lochbuehler, T. and Rohner, E. (2008). Innovative Improvements of Thermal Response
716 Tests. *Final Report,* Swiss Federal Office of Energy: Berne, Switzerland.
717 Rotta Loria, A. F. and Laloui, L. (2016). Thermally induced group effects among energy piles.
718 *Géotechnique* **67**, No. 5, 374-393.
719 Rotta Loria, A.F., Donna, A.D. and Laloui, L. (2015a). Numerical study on the suitability of
720 centrifuge testing for capturing the thermal-induced mechanical behavior of energy piles. *J.*
721 *of Geotech. Geoenviron. Eng.* **141**, No. 10, p.04015042.
722 Rotta Loria, A. F., Gunawan, A., Shi, C., Laloui, L. and Ng, C. W. (2015b). Numerical mod-
723 elling of energy piles in saturated sand subjected to thermo-mechanical loads. *Geomech. for*
724 *Energy the Environ.* **1**, 1-15.
725 Sharif, Y. U., Brown, M. J., Ciantia, M. O., Knappett, J. A., Davidson, C., Cerfontaine, B.,
726 Robinson, S. and Ball, J. (2019). Numerically modelling the installation and loading of
727 screw piles using DEM. *ISSPEA 2019*, 101-108.
728 Tang, A. M., Kalantidou, A., Pereira, J. M., Hassen, G. and Yavari, N. (2014). Mechanical
729 Behaviour of Energy Piles in Dry Sand. *Geotech. Eng. J. SEAGS AGSSEA* **45**, No. 3, 86-
730 89.
731 Takeuchi, M., Hiramoto, M., Kumagai, N., Yamazaki, N., Kodaira, A., and Sugiyama, K.
732 (1993). Material properties of concrete and steel bars at elevated temperatures. *Transactions*
733 *of 12 SMIRT* **H**, 133-138.
734 Taylor, R. N. (1995). *Geotechnical centrifuge technology*. Taylor and Francis.
735 Vitali, D., Leung, A. K., Minto, A. and Knappett, J. A. (2016). A New Model Concrete for
736 Reduced-Scale Model Tests of Energy Geo-Structures. In *Geo-Chicago,* 185-194.
737 Wang, K., Brennan, A. J., Knappett, J. A., Robinson, S. and Bengough, A. G. (2018). Centri-
738 fuge modelling of remediation of liquefaction-induced pipeline uplift using model root sys-
739 tems. *Proc. Int. J. Phy. Modell. In Geotech.* 1265-1270, UK.

740 Wood, D. M. (2004). *Geotechnical modelling*. Taylor and Francis, Abingdon.
741 Xu, Y. and Chung, D. D. L. 2000. Effect of sand addition on the specific heat and thermal
742 conductivity of cement. *Cem Concr Res.* **30**, No. 1, 59-61.
743 Yavari, N., Tang, A. M., Pereira, J. M. and Hassen, G. (2016). Effect of temperature on the
744 shear strength of soils and the soil–structure interface. *Can. Geotech. J.* **53**, No. 7, 1186-
745 1194.
746 Zhao, R., Leung, A. K., Vitali, D., Knappett, J. A. and Z., Zhou. (2020). Small-Scale Modelling
747 of Thermomechanical Behavior of Reinforced Concrete Energy Piles in Soil. *J. Geotech.*
748 *Geoenviron. Eng.* **146**, No. 4, p.04020011.
749 Zhao, R., Leung, A.K., Knappett, J.A., Robinson, S. and Brennan, A. (2021). Nonlinear Lateral
750 Response of RC Pile in Sand: Centrifuge and Numerical Modeling. *J. Geotech. Geoenviron.*
751 *Eng*. *ASCE*, **147**, No.6, p.04021031.